ARTICLE OPEN

Deep single-cell immune- and signaling profiles predict therapy response in chronic myeloid leukemia within hours

Stein-Erik Gullaksen[1,2,3]✉, Mathias Brevik[2,3,4], Erin Craig[5], Monica Hellesøy[1,2,6], Øystein Sefland[1,2,3], Ulla Olsson-Strömberg[7], Jesper Stentoft[8], Johan Richter[9], Tobias Gedde-Dahl[10], Robert Tibshirani[11,12], Sylvia K. Plevritis[11], Dominik Wolf[13], Satu Mustjoki[14,15,16], Henrik Hjorth-Hansen[17] and Bjørn Tore Gjertsen[1,2,3]✉

Chronic myeloid leukemia (CML) is effectively treated with small molecule BCR::ABL1 tyrosine kinase inhibitors (TKIs) but as in all cancers, early identification of suboptimal responders and non-responders is a challenge. Through mass cytometry analysis of peripheral blood leukocytes collected on the first day of TKI treatment, we generated high-dimensional single-cell data from de novo chronic phase CML patients enrolled in two multicenter clinical trials (clinicaltrials.gov: NCT01725204 and NCT01061177). In leukocytes, dasatinib and nilotinib inhibited intracellular signaling within 1 or 3 h after first oral dose, respectively, and each TKI had a unique signaling signature reflecting its kinase specificity profile beyond BCR::ABL1. From these data, an immune and signaling profile was constructed for each patient that predicted the treatment response (BCR::ABL1^{IS}, %) during the first 12 months of treatment. The predictive features were drug specific: response to dasatinib was dominated by leukemic burden, neutrophil maturity (pSTAT3 Y705) and immune effector activity (pERK ½ in T- and NK cells), whereas response to nilotinib was driven by the intrinsic signaling states of CD34^{+}CD38^{low}CD25^{+} LSC-like cells (cleaved caspase-3, pCRKL Y207 and STAT3 [total and Y705]). These results show that single cell immune and signaling profiles measured within hours of first dose can predict 12-month treatment response, anticipating future optimization of kinase inhibitor treatment within days rather than months.

Signal Transduction and Targeted Therapy (2026)11:499 ; https://doi.org/10.1038/s41392-026-03070-z

INTRODUCTION

Cancer treatment efficacy is evaluated only after months of therapy using bulk measurements of tumor load, which offer limited insight into the cellular effects of treatment.[1–3] In chronic myeloid leukemia (CML), a hematopoietic stem cell disease driven by the pathognomonic *BCR::ABL1* kinase gene fusion,[4–6] response is determined by measuring the residual disease through *BCR::ABL1* mRNA by a standardized RT-qPCR of peripheral blood leukocytes.[7–9] Targeting BCR::ABL1 fusion protein using tyrosine kinase inhibitors (TKIs) is highly effective, but 30–40% of patients switch their first line choice of TKI treatment.[9–13] The majority switch due to TKI intolerance (2 out of 3), while about 1 out of 3 patients switch due to a lack of response.[11] Treatment-free remission is now the therapeutic goal for younger patients with CML, currently only achieved by 20% of newly diagnosed CML patients.[14] Still, most patients require lifelong daily TKI treatment, causing treatment-related side effects and reduced quality of life with significant socioeconomic costs.[15–17]

Dasatinib, a potent sub-nanomolar dual SRC/ABL1 TKI approved for first-line treatment of CML, is readily absorbed in the GI tract and has a mean time to maximum serum concentration of 0.25–1.5 h.[18] The SRC family of kinases are efficiently inhibited by dasatinib and in vitro experiments have demonstrated that dasatinib reversibly inhibit T cell proliferation and function, in addition to NK cell function.[19–21] However, in vivo dasatinib has an immune-modulatory effect with anti-leukemic properties, including expanding subsets of cytotoxic T cells and NK cells.[22–25] Dasatinib induces contraction of stromal cells of the spleen, driving lymphocyte egress and leukocyte mobilization 1 h after oral dasatinib intake.[26–28]

Nilotinib, also a second-generation TKI approved for first line treatment of CML, has a slower mean time to maximum serum concentration of 3 h.[29] Nilotinib is a more selective inhibitor of ABL1 compared to dasatinib but show activity against other kinases including DDR-1/-2, PDGFR-α/β, KIT and CSF1R.[30] The immunological effects of nilotinib on lymphocytes are less

[1]Department of Medicine, Hematology Section, Haukeland University Hospital, Bergen, Norway; [2]K.G. Jebsen Centre for Myeloid Blood Cancer CMYC, Department of Clinical Science, University of Bergen, Bergen, Norway; [3]Centre of Cancer Biomarkers CCBIO, Department of Clinical Science, University of Bergen, Bergen, Norway; [4]Department of Chemistry, University of Bergen, Bergen, Norway; [5]Department of Biostatistics, University of Michigan, Ann Arbor, MI, USA; [6]Department of Research and Innovation, Fonna Hospital Trust, Haugesund, Norway; [7]Department of Medical Science and Division of Hematology, Uppsala University Hospital, Uppsala, Sweden; [8]Aarhus University Hospital, Aarhus, Denmark; [9]Department of Hematology, Oncology and Radiation Physics, Skåne University Hospital, Lund, Sweden; [10]Department of Hematology, Oslo University Hospital and Institute of clinical medicine, University of Oslo, Oslo, Norway; [11]Department of Biomedical Data Science, Stanford University, Stanford, CA, USA and Department of Radiology, Stanford University, Stanford, CA, USA; [12]Department of Statistics, Stanford University, Stanford, CA, USA; [13]Department of Internal Medicine V, Haematology and Oncology, Comprehensive Cancer Center Innsbruck (CCCI) and Austrian Comprehensive Cancer Network (ACCN), Medical University of Innsbruck (MUI), Innsbruck, Austria; [14]Translational Immunology Research Program and Department of Clinical Chemistry and Hematology, University of Helsinki, Helsinki, Finland; [15]Hematology Research Unit Helsinki, University of Helsinki and Helsinki University Hospital Comprehensive Cancer Center, Helsinki, Finland; [16]ICAN Digital Precision Cancer Medicine Flagship, Helsinki, Finland and [17]University IKOM, Norwegian University of Science and Technology, Trondheim, Norway
Correspondence: Stein-Erik Gullaksen (Stein.gullaksen@uib.no) or Bjørn Tore Gjertsen (bjorn.gjertsen@uib.no)

Received: 21 February 2026 Revised: 15 July 2026 Accepted: 8 September 2026
Published online: 18 November 2026

© The Author(s) 2026

explored than dasatinib. At therapeutic concentrations, nilotinib preserves key lymphoid immune functions, including T cell receptor signaling, regulatory T cell activity, and NK cell cytotoxicity.[31] The primary immune effect of nilotinib has been observed in the myeloid lineages, affecting monocyte function and maturation towards functional dendritic cells.[32–34]

The effect of TKIs on the CML leukemic stem cells (LSCs) has been extensively studied since the introduction of imatinib.[35–38] The LSCs are intrinsically resistant to TKI therapy, likely due to their quiescent nature, causing suboptimal response during treatment and relapse after TKI cessation.[39–42] Treatment response is shown to correlate with the total level of phosphorylated tyrosine measured in imatinib-treated $CD34^+$ cells in vitro.[43] Similarly, in vivo inhibition of BCR::ABL1 kinase activity in leukocytes after 7 days of imatinib and nilotinib treatment predicts response to treatment.[44] However, few studies have investigated response and the in vivo effect of TKIs on the ABL1 signaling pathway across myeloid and lymphoid cells using single-cell technologies.[45]

We have previously shown the early and direct effects of TKI therapy on both immune and leukemic cells from patients with CML.[39,46–48] High dimensional mass cytometry analysis suggested that single-cell immune- and signaling profiling may distinguish optimal responders from sub-optimal responders.[46,48] Therefore, we hypothesize that it is possible to generate response prediction already hours after the first dose of TKI. We tested this hypothesis in single peripheral blood cells (PB) from two clinical trials of de novo chronic phase CML. Analysis of PB collected before and within hours after starting dasatinib or nilotinib therapy demonstrated that the first TKI dose inhibited intracellular signal transduction. Furthermore, single cell profiles of PB collected at baseline and hours after the first TKI dose in both studies effectively predicted therapy response the first year of TKI treatment.

RESULTS

Experimental design and mass cytometry-derived absolute counts

To investigate the immediate effects of dasatinib (100 mg once daily, NordCML007; NCT01725204) and nilotinib (300 mg twice daily, ENEST1st; NCT01725204) on immune cells, we collected up to four longitudinal peripheral blood samples (PB, $n = 229$) from each patient with de novo chronic phase CML ($n = 81$) (Fig. 1a). The leukocytes were fixed immediately following blood draw using BD Phosflow Lyse/Fix following vendor's protocol to preserve intracellular signaling states for analysis by mass cytometry. Paired PB samples were collected from patients ($n = 32$) in the NordCML007 trial before and 1 h after the first per oral dasatinib dose on day one (t0, t1), and after three months of daily dasatinib, before and 1 h after the daily per oral dosing (t2, t3). Similarly, leukocytes were collected and preserved from patients ($n = 49$) in the ENEST1st trial before and 3 h after the first nilotinib dose (et0, et1) on day one. The different intervals between pre- and post-treatment samples reflected the median time to maximum serum concentration of dasatinib (~1 h) and nilotinib (~3 h). The patient samples, together with healthy donor samples (HDPB; $n = 17$, HDBM; $n = 19$), were stained with a panel of 43 metal-conjugated antibodies enabling deep immunophenotyping and profiling of BCR::ABL1-related signaling pathways. In addition, cationic granular proteins of eosinophils were labeled by cisplatin ($^{Pt}195$) through charge-based interactions[49] and used in immunophenotyping alongside antibody-derived data (Supplementary Text). We acquired high-dimensional data from a total of 44 million single cells from patient and healthy donor samples. Firstly, the main immune populations were identified using Cytosplore (HSNE[50]) clustering and secondly, a selection of these populations were re-clustered using PARC[51] and a tailored selection of markers to further increase phenotypic resolution (Fig. 1b, c). After manual curation and annotation of the clusters, 37 unique immune populations were identified. The data from each clinical trial were analyzed independently but following the same bioinformatic pipeline, and no batch effect correction was performed (Fig. 1d).

Differential testing using proportions of immune populations (%, compositional data) may be biased, as a change in the absolute counts of one cell type (or cluster) will affect the proportions of all clusters.[52] To avoid bias from dasatinib-induced acute but transient lymphocytosis[27,28] affecting cluster proportions, we used routine white blood cell (WBC) absolute counts (10^9 cells/L) obtained at study visits to estimate absolute counts from mass cytometry cluster proportions (%). The mass cytometry-derived absolute cluster counts (hereafter eCounts) and routine differential absolute counts were closely correlated in both clinical trials (Supplementary Text and Supplementary Fig. 1). We next used $\log_2$-transformed ratios of eCounts to assess immune cell mobilization following per oral dasatinib and nilotinib (Fig. 1e). One hour after dasatinib dosing, the most pronounced mobilization was observed in B cells and subsets of NK cells and monocytes, particularly after 3 months of treatment, with cytotoxic T cell subsets showing more modest changes. A similar pattern was observed after the first dasatinib dose on day one, although the $\log_2$-ratio of mobilization was generally lower and did not include monocyte subsets. In contrast, nilotinib treatment did not induce mobilization of any major immune cell populations, as has been previously observed.[27] The only exception was a modest but statistically significant reduction in non-classical monocytes 3 h after the first dose.

Longitudinal deep immune and signaling profiles of CML compared to healthy donors

We next wanted to characterize the dysregulation of PB cells from CML patients before the start of treatment. We therefore compared the composition of immune populations (eCounts), the BCR::ABL1-related signaling pathways and immune-activation state (CD38 and HLA-DR expression) with HDPB.

Since the myeloid cells are expected to express the BCR::ABL1 fusion-protein driving the CML, this cell compartment was analyzed first. We found, as expected, that samples from untreated CML patients in both trials (t0 and et0) exhibited significantly increased eCounts of most myeloid cell populations, including basophils, eosinophils, neutrophil subsets, classical monocytes, and dendritic cells compared to healthy donor controls (Fig. 2a, b). The level of pSTAT3 Y705 in the neutrophil subsets was significantly reduced, indicating that these cells, even in seemingly mature and CD16 expressing neutrophils, were less mature than in the phenotypically similar healthy donor counterparts (Fig. 2c, d).[53] Notably, the global level of phosphorylated tyrosine residues (clone: p-Tyr-100) was significantly increased in the basophils. Following three months of dasatinib treatment in the NordCML007 trial, both signaling state and eCounts in most myeloid populations were normalized and comparable to controls. There were, however, some exceptions with a significantly reduced eCount of neutrophils, basophils, monocytes, and dendritic cells, which is consistent with myelosuppression, a well-known side effect of TKI treatment.[54,55] Neutropenia, both grade 2 and 3–4, was detected in 20% of patients in the NordCML007 trial the first 12 months of treatment.[56]

Although the CML-related dysregulation in the myeloid populations in both cohorts was similar before starting treatment, we found that the lymphocyte compartment was more dissimilar. In untreated samples from patients enrolled in the NordCML007 trial, we observed an increased eCount of several lymphocyte subsets, including $CD8^+$ central memory (CM) T cells and regulatory T cells (Tregs). Many T cell subsets also exhibited significantly elevated levels of both pCREB S133 and pSTAT3 Y705, and a lower level of pSTAT5 Y694 was observed in both T and NK cells. Overall, we did not make the same observations in the patients in the ENEST1st

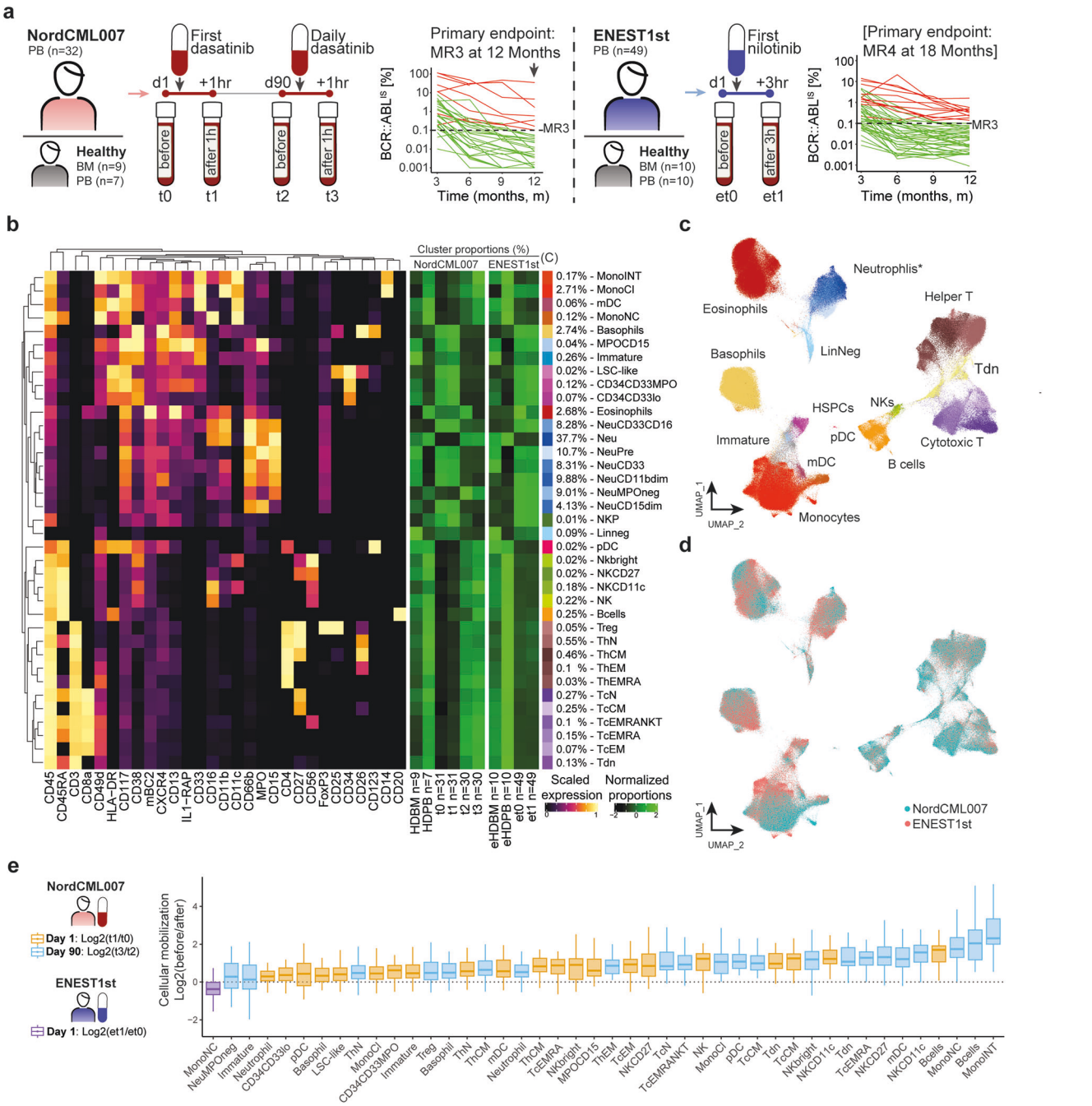

Fig. 1 Experimental design and leukocyte mobilization. **a** Experimental design of longitudinal peripheral blood (PB) sampling and BCR::ABL1^{IS} monitoring during the first year of treatment in de novo patients enrolled in the clinical trials NordCML007 and ENEST1st. Healthy donor PB (HDPB) and bone marrow (HDBM) samples were analyzed alongside each cohort of longitudinal patient samples. Green and red lines show patients with BCR::ABL1^{IS} above or below 0.1% after 12 months, denoting responders and non-responders, respectively. **b** Heatmap (left) showing the normalized median expression of proteins used for deep immunophenotyping in 37 immune populations identified by HSNE and PARC clustering. The right green heatmaps show normalized proportions (%) of each cluster in longitudinal patient and healthy donor samples. **c** Uniform manifold approximation and projection (UMAP) representation of single cells from both patients and healthy donors colored by immune population as in **b**. *The neutrophil clusters were sub-sampled to 10% prior to UMAP-analysis to improve visualization. **d** UMAP as in **c**, but colored by clinical trial dataset (NordCML007, ENEST1st). **e** Log_2 fold change in eCounts of immune populations between t0 and t1, t2 and t3 (NordCML007), and et0 and et1 (ENEST1st), for each patient. Only populations with a significant FDR-adjusted *p*-value (paired *t*-test) are shown

trial, except in an increased eCount of NK precursors (CD56^{-}) and a significantly elevated level of pSTAT3 Y705 in Naïve and CM T helper cells. The eCounts from the HDPB samples collected alongside the NordCML007 ($n = 7$) and ENEST1st (n = 10) patient samples were highly consistent, with no significant group-wise differences in eCounts (Supplementary Fig. 2).

Similarly to the myeloid cell subsets after three months of daily dasatinib in the NordCML007 trial, the eCounts of multiple lymphocyte subsets were significantly reduced after dasatinib treatment, most notably B cells, CD56^{++} NKs, CD4^{+} Naïve T cells, and Tregs. Furthermore, a sustained elevation in pCREB S133 and pSTAT3 Y705 levels, along with a reduced pSTAT5 Y694 in T and

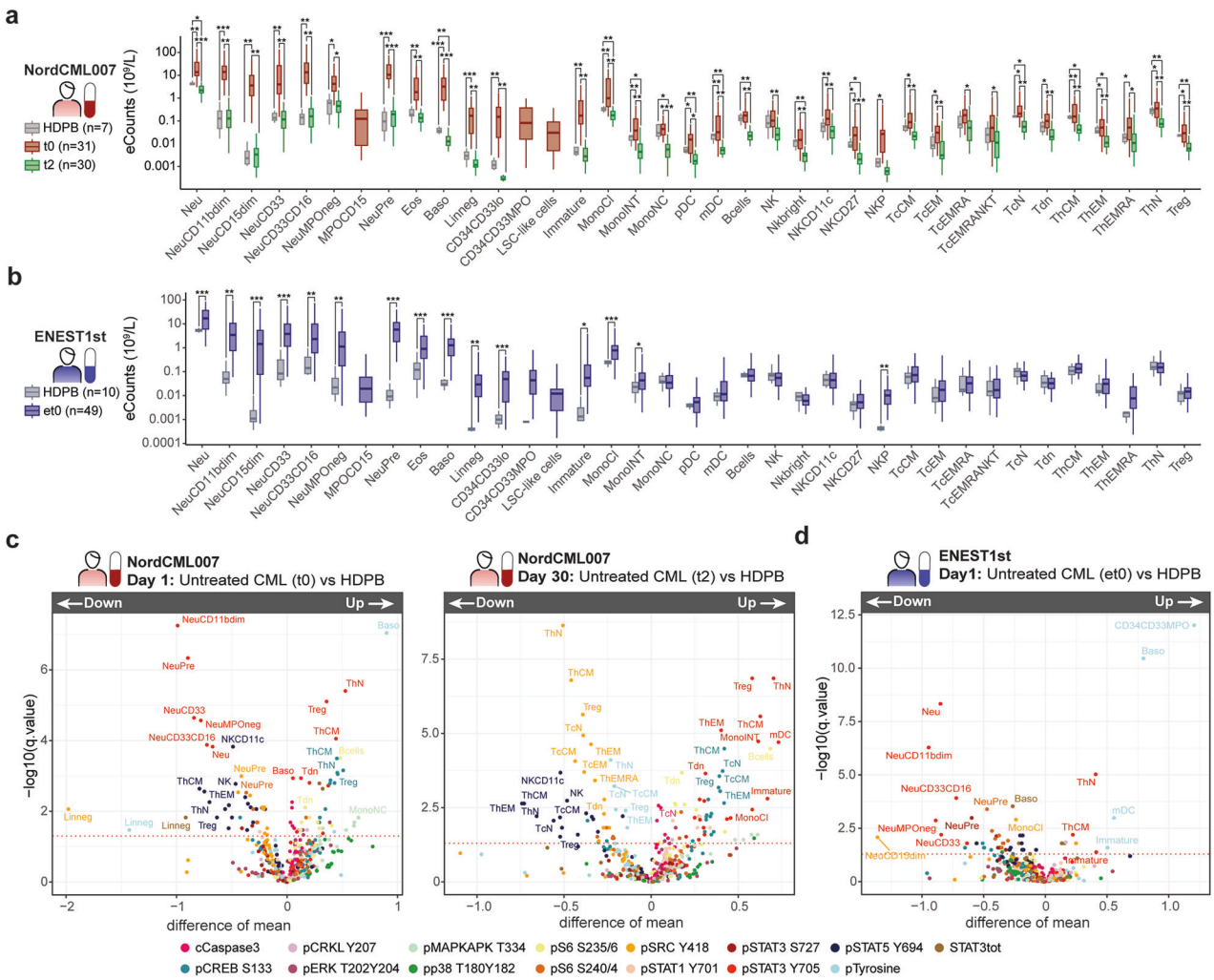

Fig. 2 Longitudinal deep immune and signaling profiles of CML. **a** Boxplots showing eCounts of immune populations from patient samples before treatment: dasatinib day 1 (red) and day 90 (green) from NordCML007 trial. Healthy donor peripheral blood (HDPB) samples shown in gray. Statistical comparisons used false discovery rate (FDR) adjusted grouped two-sided *t*-test (patient vs. HD samples) and paired two-sided *t*-test (day 1 vs. day 90). **b** Same as in **a** but showing eCounts of immune populations from patients in the ENEST1st trial, before first nilotinib treatment on day 1(et0, blue). Healthy donor peripheral blood (eHDPB) samples shown in gray. **c** Average difference in intracellular signaling states between HDPB and patient samples for each cell type, with FDR adjusted grouped two-sided *t*-test (patient vs. HDPB) on the y-axis. Differences are shown for samples collected before dasatinib treatment on day 1 (t0, left), or on day 90 (t2, right), from patients in the NordCML007 trial. **d** Same as in **c** but differences are shown for samples collected before dasatinib treatment on day 90 (t2) from patients in the NordCML007 trial, i.e., patient vs HDPB All comparisons are based on grouped *t*-tests with for multiple testing. Significance levels are indicated as follows: $p_{adj} \leq 0.05$: *, $p_{adj} \leq 0.01$: **, $p_{adj} \leq 0.001$: ***, $p_{adj} \leq 0.0001$: ****

NK cells was observed, in addition to a decrease in pSRC Y418. The neutrophils showed a clear increase in pSTAT3 Y705, but not pSTAT3 S727, after three months in the various neutrophil populations, compared to the level of healthy donor neutrophils.

Finally, we investigated the level of CD38 and HLA-DR on T and NK cells as a measure of their activation states (Supplementary Fig. 3). In both patient cohorts, a significantly increased CD38, but not HLA-DR, expression in T helper effector memory (ThEM) cells and reduced expression on Naïve T helper cells were found. The CD38 expression on Naïve T helper cells was further reduced after three months of treatment with dasatinib, while the increased level on ThEM was normalized.

Signaling kinetics of TKIs after first per oral dosing

Having confirmed that our early longitudinal sampling captured dasatinib-induced changes after 1 h, exemplified by acute immune cell mobilization (Fig. 1e), we next investigated intracellular signaling changes induced by TKI treatment. We began by examining global levels of phosphorylated tyrosine residues in basophils and $CD34^+$ populations (Fig. 3a, b). Compared to HDPB samples, relative phosphorylated tyrosine levels were 3.26 ± 0.31 and 5.68 ± 1.14-fold higher in basophils from untreated CML patients, for nilotinib and dasatinib, respectively, consistent with constitutive BCR::ABL1 activity driving elevated tyrosine phosphorylation. Strikingly, in both patient cohorts, we observed a highly significant decrease in phosphorylated tyrosine 1 h after the first dasatinib ($p_{adj} = 2.42 \times 10^{-11}$) and 3 h after the first nilotinib tablet ($p_{adj} = 8.64 \times 10^{-11}$). When analyzing the correlation between immune- and signaling features we found that the baseline and change in phosphorylated tyrosine were highly correlated in patients treated with dasatinib, but not in patients treated with nilotinib (Supplementary Text). Interestingly, in the basophils after 3 months of daily dasatinib treatment, dasatinib also induced a significant ($p_{adj} = 1.32 \times 10^{-4}$) reduction of phosphorylated tyrosine residues.

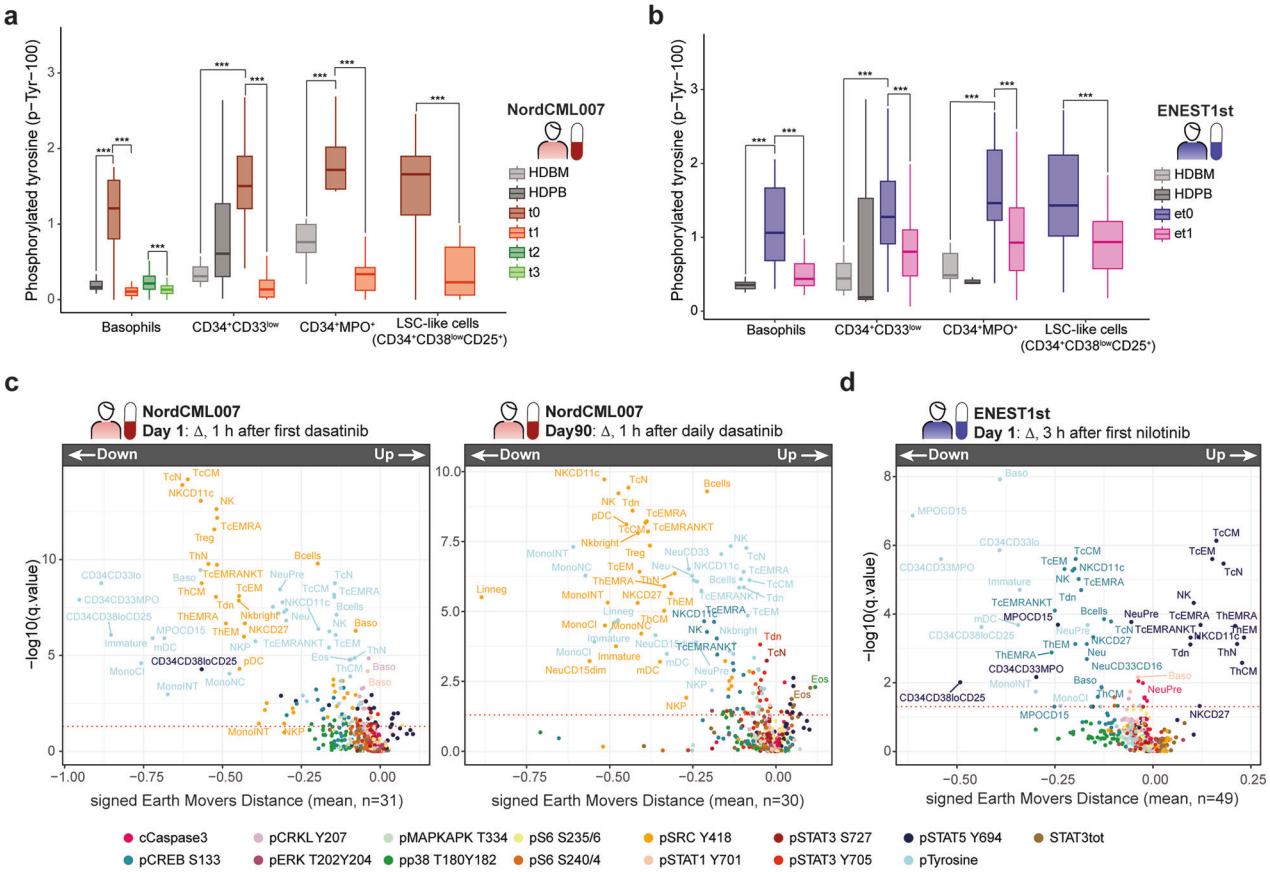

Fig. 3 TKIs inhibits signaling hours after first per oral dosing. **a**, **b** Boxplots show the 75th percentile measurement of phosphorylated tyrosine residues using the P-Tyr-100 antibody clone in basophils and CD34⁺ cell clusters from patients with CML across longitudinal patient samples from patients treated with dasatinib and nilotinib, respectively. The 75th percentile of phosphorylated tyrosine residues from same populations from HD healthy donor peripheral blood (HDPB) and bone marrow (HDBM) samples are shown in shades of gray. **c**, **d** Signed Earth Movers Distance (sEMD) measures of changes in signaling 1 h (dasatinib; day 1; left and day 90; right) and 3 h (nilotinib) after first dose of tyrosine kinase inhibitor. These sEMD measures of changes of signaling have been visualized with an FDR-adjusted and paired *t*-test analysis using 75th percentiles on the y-axis. All comparisons are based on paired *t*-tests with false discovery rate (FDR) correction for multiple testing. Significance levels are indicated as follows: $p_{adj} \leq 0.05$: *, $p_{adj} \leq 0.01$: **, $p_{adj} \leq 0.001$: ***, $p_{adj} \leq 0.0001$: ****

The level of tyrosine phosphorylation was higher in the untreated patient CD34⁺ populations compared to both the basophils in the patient samples and CD34⁺ populations from healthy donors, suggesting BCR::ABL1 expression.[57,58] Additionally, we also observed a highly significant reduction in phosphorylated tyrosine 1 h after the first dasatinib and 3 h after the first nilotinib tablet in the CD34⁺ populations, including the LSC-like cells (dasatinib: $p_{adj} = 1.37 \times 10^{-7}$, nilotinib: $p_{adj} = 1.22 \times 10^{-5}$).

To characterize the broader effect of the TKIs on intracellular signaling associated with BCR::ABL1 we used signed earth movers distance measure (sEMD) combined with an FDR-adjusted and paired two-sided *t*-test of 75th percentile measurements in Fig. 3c, d. Similar to basophils and LSC-like cells, we observed a broad reduction in phosphorylated tyrosine levels across most immune populations, with the most pronounced effects in myeloid lineage cells (monocytes and other CD34⁺ populations) compared to lymphoid cells. A hallmark of BCR::ABL1-inhibition is the downregulation of pSTAT5 Y694 in CML stem cells and cell lines.[59,60] In our patient samples, hours following per oral TKI dosing, we observed a significant inhibition of pSTAT5 Y694 in all three CD34⁺ cell populations in patients treated with both dasatinib and nilotinib, with the most prominent downregulation observed in the LSC-like cells. In a population of cells with a phenotype resembling pre-neutrophils (CD66b⁺CD34⁻CD117⁺CD38⁺CD49d⁺) we observed a significant reduction in pSTAT5 Y694 in both dasatinib and nilotinib treated patients.[61–63] Dasatinib treatment also resulted in a modest but significant downregulation of pCRKL Y207, pSTAT1 Y701 and pSRC Y418 in basophils, similar previous observations 3 h after first nilotinib,[46] and in most neutrophils populations (Supplementary Fig. 4).

In the lymphoid compartment, we measured a downregulation of pSRC Y418 following dasatinib treatment in most cell subpopulations, but most strikingly in T and NK cell subsets. This is likely reflecting dasatinib inhibition of SRC-family kinases and not ABL1, and no regulation of pSRC Y418 was observed in nilotinib-treated patients. Interestingly, inhibition of pSRC Y418 was also readily measurable 1 h after dasatinib dosing in samples collected after 3 months of treatment. In the nilotinib-treated patients (Fig. 3d) we were able to validate using mass cytometry previous results showing an increase in pSTAT5 Y694[46] alongside a reduction in pCREB S133 in T and NK cells.

Responders to dasatinib and nilotinib are predicted by unique sets of immune features

We next asked whether our immune features were predictive of treatment response as measured by *BCR::ABL1* mRNA levels (BCR::ABL1^{IS}) every 3 months during the first year of treatment. To enable direct comparison between the dasatinib and nilotinib cohorts, we standardized our analysis to immune features derived from equivalent early timepoints: baseline measurements before TKI initiation (t0 for dasatinib, et0 for nilotinib) and acute

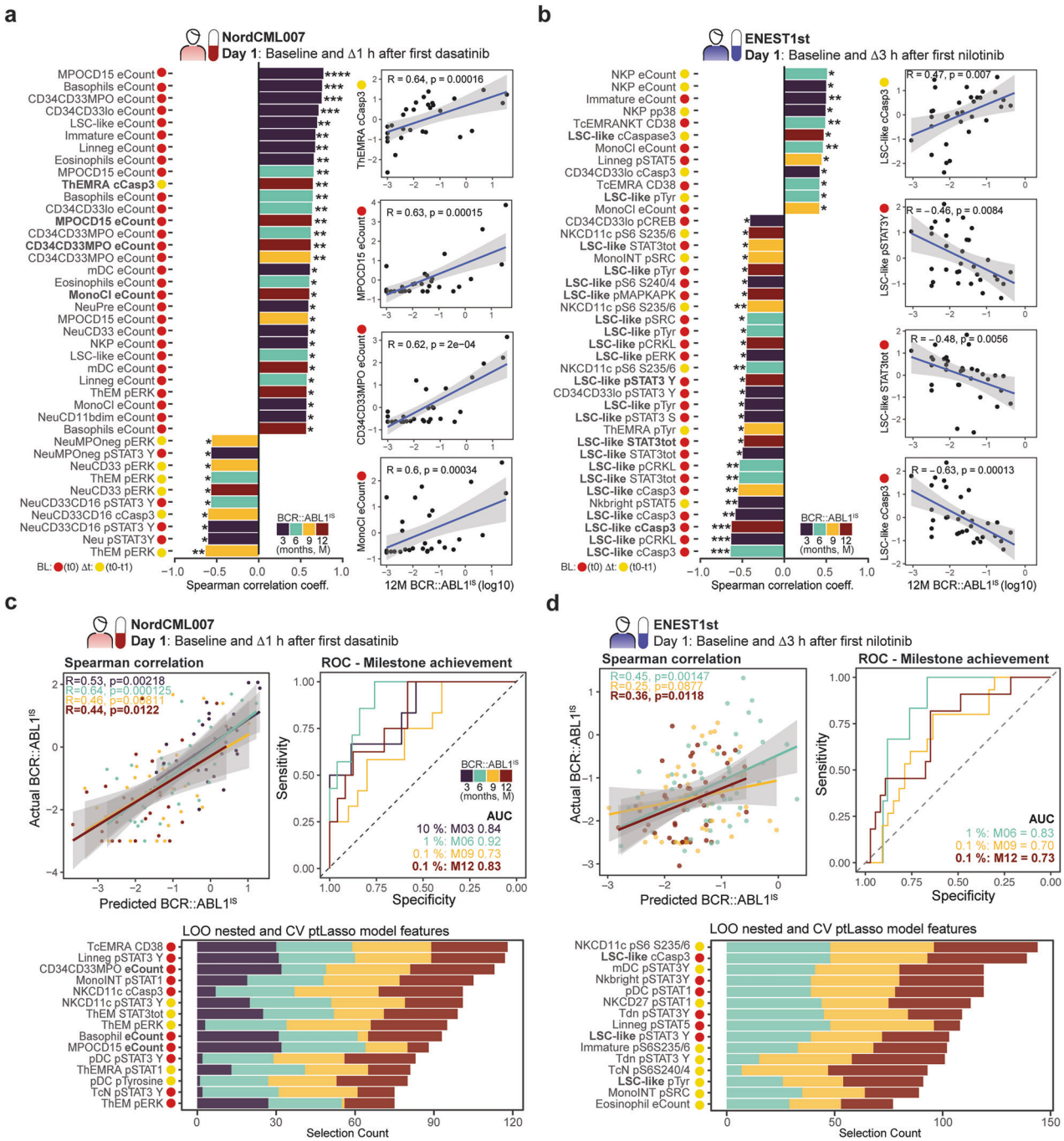

Fig. 4 Responders to dasatinib and nilotinib are defined by unique sets of immune features. **a**, **b** Top 30 Spearman correlations (ranked by correlation coefficient R) between immune features and BCR::ABL1^{IS} [%] levels at 3-, 6-, 9-, and 12-months post-treatment initiation in dasatinib-treated patients. Immune features extracted from baseline samples (red, t0/et0) and changes from baseline to 1 h (dasatinib) or 3 h (nilotinib) after first TKI dose (yellow). **c**, **d** Predictive modeling of BCR::ABL1^{IS} using pretrained LASSO logistic regression on the same data as above. Model performance evaluated by Spearman correlation between predicted and observed BCR::ABL1^{IS} and Receiver operating characteristics and Area under the Curve (AUC) statistics for classifying responders at milestone timepoints (BCR::ABL1^{IS} ≤ 10% at 3 months, ≤1% at 6 months, ≤0.1% at 9 and 12 months). Selection frequency of immune features during the double-layered leave-one-out nested and cross-validated pretrained LASSO analysis

treatment-induced changes measured one or 3 h after the first dose (Δ, t1–t0; Δ, et1–et0).

To get an overview of the correlated immune features, we first performed Spearman correlation analysis of immune features and BCR::ABL1^{IS} measurements the first year of treatment in each cohort. Overall, the number and strength of significantly correlated immune features in nilotinib-treated patients were lower than in the dasatinib-treated patients (Fig. 4a, b). Features related to immune activation (pERK ½ in ThEM cells) and high leukemic burden at baseline (t0, eCounts of myeloid and CD34^{+} cells and pSTAT3 Y705 in neutrophils) were the dominant immune features correlating with response to dasatinib. In contrast, in nilotinib-treated patients immune features correlating response were largely driven by the LSC-like cell population. Specifically,

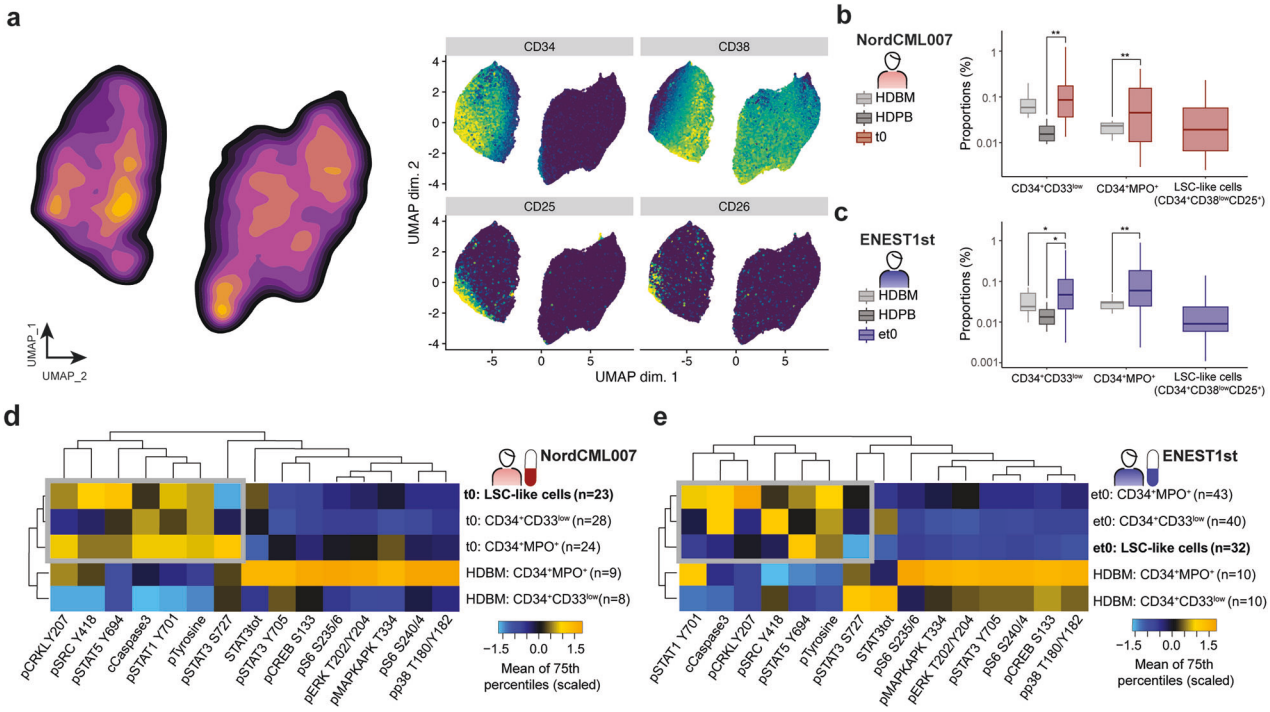

Fig. 5 CML stem-like cells display elevated levels of phosphorylated tyrosine residues and pSTAT5 Y694. **a** UMAP embedding of isolated CD33$^+$ intermediate and CD34$^+$ cells (left). Single-cell expression of selected surface markers with each marker scaled independently (right). **b**, **c** Proportions (%) of CD34$^+$ cell clusters in samples collected before TKI treatment on day 1 from patients enrolled in the NordCML007 trial or ENEST1st trial. **d**, **e** Heatmaps showing the scaled average 75th percentile expression of intracellular signaling markers associated with BCR::ABL1 signaling across the CD34$^+$ cell clusters in the NordCML007 trial or ENEST1st trial. In both (**b**–**d**), healthy donor peripheral blood (HDPB) and bone marrow (HDBM) samples are shown for comparison. All comparisons are based on group *t*-tests with false discovery rate (FDR) correction for multiple testing. Significance levels are indicated as follows: $p_{adj} \leq 0.05$: *, $p_{adj} \leq 0.01$: **, $p_{adj} \leq 0.001$: ***, $p_{adj} \leq 0.0001$: ****

baseline levels of cleaved Caspase-3, pCRKL Y207 and STAT3 (total and phosphorylated) in LSC-like cells before starting treatment with nilotinib were negatively correlated with BCR::ABL1^{IS}. Whereas the increase in cleaved Caspase-3 LSC-like cells 3 h after the first nilotinib tablet was positively correlated with BCR::ABL1^{IS}. In addition to the LSC-like population, the change in eCounts of NK progenitors (NKP) after 3 h and baseline classical monocytes (MonoCl) were all positively correlated with BCR::ABL1^{IS}.

To move beyond pairwise associations, we built a predictive model of treatment response using a pretrained LASSO variant (ptLasso). LASSO supports multivariate modeling while selecting a minimal set of informative features, producing interpretable, generalizable models. Pretraining captured relationships common to all BCR::ABL1^{IS} outcomes in the first treatment year, followed by month-specific fine-tuning to enhance individual predictions.[64] Model fitting and performance were evaluated with leave-one-out nested cross-validation to ensure unbiased estimates.[65] Using early immune and signaling features, we trained models within each clinical trial to predict BCR::ABL1^{IS} every three months during the first year of treatment. Model performance, evaluated by Spearman correlation, revealed strong agreement between predicted and observed BCR::ABL1^{IS} values in both NordCML007 (12 months, $R = 0.44$, $p = 1.22 \times 10^{-2}$) and ENEST1st (12 months, $R = 0.36$, $p = 1.18 \times 10^{-2}$). We further assessed classification performance by predicting optimal versus suboptimal responders at each milestone timepoint (BCR::ABL1^{IS} ≤ 10% at 3 months, ≤1% at 6 months, and ≤0.1% at 9 and 12 months; Fig. 4c, d). The models achieved high discriminative performance, with AUCs of 0.83 (NordCML007) and 0.73 (ENEST1st) at 12 months. Compared head-to-head with established clinical risk scores, ptLasso predictions showed consistently superior Spearman correlation with observed BCR::ABL1IS across all 3-monthly milestones in NordCML007, and comparable or superior performance to the ELTS score in ENEST1st (Supplementary Figs. 5 and 6, respectively). Notably, many of the top-ranked features selected by the model overlapped with those identified in the Spearman analysis, reiterating that the features predicting the response to dasatinib and nilotinib are different.

CML Stem-like cells are characterized by increased levels of phosphorylated tyrosine residues, including pSTAT5 Y694

Given that LSC-like cells and their intrinsic signaling states emerged as dominant predictive features specifically in nilotinib-treated patients, in contrast to the leukemic burden and immune activation features that predicted dasatinib response, we investigated whether this difference reflected pre-existing biological heterogeneity between the two patient cohorts. In the UMAP embedding of cells from patients in both cohorts and healthy donors (Fig. 1c), we noticed two islands of cells expressing CD33 close to the monocyte subsets, where the most distant cells all expressed CD34. These intermediate and CD34-expressing cells were subjected to a new UMAP analysis to evaluate their immunophenotypic composition in detail (Fig. 5a). This UMAP analysis clearly showed two distinct islands of cells, separated by CD34 expression. The CML leukemic stem cell markers CD25 and CD26 were co-expressed on a subset of CD34-expressing cells with lower levels of CD38, and these cells were highly enriched in the LSC-like population (CD34$^+$CD38^{low}CD25$^+$). These cells were 47-fold more frequent in leukemic samples compared to healthy donor samples. The median number of LSC-like cells (CD34$^+$CD38^{low}CD25$^+$) acquired per patient was 21 (range 1–241) in the NordCML007 cohort and 12 (range 1–383) in the ENEST1st cohort (Supplementary Data S1 and Supplementary Fig. 7). The proportions of the three CD34$^+$ populations were comparable between the two cohorts of patients (Fig. 5b, c).

Next, we characterized the LSC-like population by comparing the basal state of intracellular signaling in all $CD34^+$ populations where more than 5 cells were detected. For each of the intracellular markers and each $CD34^+$ population, we calculated the average 75th percentile expression for healthy donor BM samples and the untreated CML samples (Fig. 5d, e). We found that the signal transduction profiles of $CD34^+$ populations from untreated CML patients were clearly unique compared to phenotypically similar cells from HDBM, and consistent between patient samples from the two trials. As expected in cells expressing BCR::ABL1, the $CD34^+$ patient populations all had a higher level of phosphorylated tyrosine residues compared to the healthy clusters. The CD25 and CD26 expressing LSC-like cells were further distinct by a higher level of pSTAT5 Y694 in addition to a lower level of pSTAT3 S727. Interestingly, cleaved caspase 3 was also lowest in the LSC-like cells.

DISCUSSION

There is a fundamental temporal disconnect between the biology of targeted cancer therapy and current response evaluation methods. While pharmacodynamic studies demonstrate that cellular responses to targeted therapy can be measured within hours through intracellular signaling monitoring,[46,48,66,67] clinical response evaluation in CML relies on assessments performed every three months ($BCR::ABL1^{IS}$).[9] Here, we demonstrate that a unique set of predictive immune features for dasatinib or nilotinib captured within hours of initiating TKI treatment can predict long-term therapeutic outcomes at the individual patient level.[68–70] These rapid, single-cell measurements of intracellular signaling states across distinct cellular subsets, integrated with tumor- and immune cell composition, reveal coordinated patterns of TKI response. Our findings represent a novel approach for ultra-rapid response assessment of targeted cancer therapy.

Several factors influence the on-target effects of TKIs in patients, including the TKI dose ingested, concomitant medications, and pharmacokinetic variables such as GI absorption and hepatic metabolism.[71] When we compared the reduction in basophil tyrosine phosphorylation levels after the first dose of TKI, we observed differences in patients treated with dasatinib and nilotinib. One hour after dasatinib ingestion, residual basophil tyrosine phosphorylation was below or comparable to HDPB (mean ratio: 0.55 ± 0.12). In contrast, patients treated with nilotinib exhibited higher residual tyrosine phosphorylation compared to HDPB (mean ratio 1.57 ± 0.17). This likely reflects the twice-daily dosing of nilotinib (300 mg BID), as our peripheral blood samples were collected after only one dose. This demonstrates that we can quantify the extent of TKI inhibition of intracellular signaling in distinct cellular subsets.

The interactions between leukemic cells and the immune system are critical determinants of treatment outcomes in cancer.[72–74] In dasatinib-treated patients, we find that immune features measured within hours that correlated with treatment response were dominated by leukemic burden, neutrophil maturity (pSTAT3 Y705), and immune cell activity (pERK ½ in T-and NK cells). These features reflect the broad kinase inhibition profile of dasatinib beyond ABL1, particularly its activity towards SFK-kinases, and provide additional evidence for the importance of dasatinib's immunomodulatory mechanisms in cells.[23,25,75,76] Huuhtanen et al. analyzed samples from the same NordCML007 trial patients using flow cytometry, scRNA-seq, and functional assays on cryopreserved PBMCs.[22] Although they focused primarily on cellular proportions and functional changes following IFN-α addition to dasatinib therapy, baseline $CD107^+GZMB^+$ NK cells correlated with $BCR::ABL1^{IS}$ after 12 and 18 months. This is consistent with a feature identified in our machine learning model, where changes in pSTAT3 Y705 in $CD11c^+$ NK cells correlate to response at 12 months.

In contrast, the effect of nilotinib was predominantly centered on $CD34^+CD38^{low}CD25^+$ and $CD26^+$ LSC-like cells and their intrinsic signaling states (cCaspase-3, STAT3 [total and Y705], and global tyrosine phosphorylation changes). The high selectivity of nilotinib to BCR::ABL1, and consequently its minimal immunomodulatory activity, suggests that nilotinib treatment outcomes more strongly depend on the LSCs' survival pathways alone.[77,78] When comparing LSC-like cells between the dasatinib- and nilotinib-treated patients, we found that the basal intracellular signaling states were highly comparable (Fig. 5). When machine learning approaches were applied to the same data to predict individual patient outcomes during the first year of treatment, there was substantial overlap between the immune features selected by the model and those identified by Spearman correlation analysis.

The mechanistic basis of non-response likely differs between the two TKIs studied. In dasatinib-treated patients, the immune features predictive of suboptimal response suggest that insufficient immune effector response, rather than failure of on-target BCR::ABL1 inhibition. This is consistent with the established role of NK- and cytotoxic T cell function in determining TKI response and treatment-free remission in CML.[72–74] In contrast, responses to nilotinib were predicted by LSC-like cell apoptotic priming (cCaspase-3) and STAT3 signaling, which is consistent with resistance arising from the intrinsic survival pathways of LSCs that are maintained independently of BCR::ABL1 kinase activity.[77,78] These pathways, including JAK1/STAT3, metabolic adaptation, and niche-dependent signals, are not targeted by nilotinib, and their baseline activity may determine residual persistence. Direct measurement of pharmacodynamic BCR::ABL1 inhibition at the single-cell level in these populations remains an important future experiment to formally dissect on-target from off-target mechanisms of resistance. Collectively, these findings suggest that baseline characteristics and single-cell immune and signaling profiles could inform personalized selection between dasatinib and nilotinib. For example, patients with elevated LSC-like cell apoptotic priming and STAT3/pCRKL signaling may be better candidates for nilotinib, while patients dominated by high leukemic burden and active immune effector features may benefit more from dasatinib given its broader immunomodulatory kinase profile. We hypothesize that our prediction of response to TKI could guide initial TKI selection and increase the proportion of patients eligible to treatment discontinuation; a hypothesis that warrants testing in prospective clinical trials. First-year molecular response kinetics (specifically the depth and rate of $BCR::ABL1^{IS}$ decline) are established predictors of sustained treatment-free remission (TFR),[79] and immune and signaling features that capture those kinetics within hours of treatment initiation may therefore carry indirect predictive information relevant to TFR eligibility or success—available far earlier than current monitoring allows.

Translating this approach into clinical practice will require several steps. Sample preservation workflows should be standardized around recently available commercial fixation tubes (e.g., Smart Tubes, Cytodelics), that significantly reduces the processing time after blood draw to a 10 min incubation with stabilization buffer before storage at −80 °C. A further barrier to clinical implementation lies in the analytical platform itself. Although mass cytometry enables deep immune and signaling profiling, it is costly, technically demanding, and not widely available outside specialized laboratories. By contrast, flow cytometry is already an established diagnostic tool in most hospitals, underscoring the need to bridge advanced discovery-level analyses with clinically deployable tools. The most pragmatic solution would be reducing the panel to the smallest set of features with robust predictive value, readily implementable on flow cytometry platforms already available to most clinics. However, such simplification would sacrifice breadth, as other TKIs likely carry their own unique predictive immune- and signaling signatures not captured by

reduced panels. An alternative is to retain the full mass cytometry workflow: with peripheral blood samples stabilized at bedside and shipped overnight and analyzed within days centrally using advanced single-cell deep immune and signaling and sophisticated bioinformatical pipelines. The feasibility, turnaround time, and cost-effectiveness of both approaches require prospective evaluation. Most importantly, a prospective clinical trial should be designed to test whether reassigning patients to an alternative TKI based on their hours-post-dose deep single-cell immune and signaling profiles improves rates of deep molecular responses and possibly TFR. The present findings establish the biological rationale and provide an analytical framework for such trials.

This study has some important limitations. First and foremost, this study has a relatively small sample size. In ENEST 1st clinical trial the collection of samples was planned from 200 patients, but we only obtained usable samples from approximately 50 patients across European centers. In NordCML007, we collected and analyzed samples from 32 out of 40 patients enrolled in centers in the Nordic countries. These samples were preserved using the BD Lyse/Fix buffer (BD Phosflow; 37 °C water bath, centrifugation, storage −80 °C), a method specifically developed and validated to preserve intracellular phosphorylation states in leukocytes from peripheral blood. In both trials, the biological sampling window was the primary temporal focus, 1-h post-dose in NordCML007 and 3 h in ENEST1st clinical trials. However, delays in sample processing of collected samples, including the time from venipuncture to start of Lyse/Fix processing, could influence signal transduction and add noise to our analysis. Although all sites were instructed to minimize the time between venipuncture and start of Lyse/Fix processing, variability across clinical sites represents a limitation. A realistic "bedside-to-report" timeline for the present study and planned future studies is shown in Supplementary Fig. 8. Recently, more simple preservation buffers have become commercially available (Smart tubes, Cytodelics) significantly easing the sample preservation to a 10 min protocol to be performed following blood draw. We expect new sampling tube technology to significantly increase the feasibility of larger studies of immediately preserved full blood.

The peripheral blood samples were collected from patients in two clinical trials with different inclusion criteria for prior treatments allowed before starting the study drug. The NordCML007 trial only allowed prior hydroxyurea for up to 60 days, whilst ENEST1st allowed TKI treatment up to 3 months and hydroxyurea for up to 6 months. In our cohort of patients from the ENEST1st trial, only one patient had received prior TKI-treatment and there was no significantly increased duration (days) of hydroxyurea (Supplementary Fig. 9) compared to the NordCML007 trial (Wilcoxon rank sum test $p = 0.259$).

Systematic technical variation from sample preservation, antibody labeling and instrumentation is a significant hurdle for clinical application of longitudinal studies using high-dimensional single-cell technologies. We partly mitigated this in our sample preparation by staining all samples on the same day using the same frozen and aliquoted antibody master mix and storing the labeled samples at -80°C for data acquisition. The data from the NordCML007 samples were acquired on a Helios mass cytometer within weeks, while ENEST1st samples were collected a year later using a CyTOF XT instrument. Despite this, we observed a minimal batch effect (Fig. 1d, Supplementary Fig. 2) and chose to analyze the data without any normalization. This work lays the ground for future clinical implementations where a single longitudinally collected sample can be analyzed independently to generate clinically meaningful data for response prediction without requiring normalization to large reference cohorts or standardization to a single instrument platform.

In conclusion, we have found that dasatinib and nilotinib induce changes in intracellular signaling hours after the first per-oral dose, allowing for a rapid therapy optimalization. Methodologically, it is feasible to measure the effects of targeted treatment by modifications of protein kinases within minutes or hours after the drug exposure.[80,81] We suggest that this should be performed with single-cell resolution to secure information from TKIs with different profiles of target inhibition. Single cell immune- and signaling profiling may in this way be developed into a next-generation white blood cell count, providing a precision in diagnostics that matches the precision of targeted therapy. Independent prospective validation in a new patient cohort using a pre-specified and simplified immune feature set remains the critical next step. Such a study would determine whether early single-cell immune profiling can be integrated into clinical decision-making algorithms to guide upfront TKI selection.

MATERIALS AND METHODS

Patients and healthy donor samples

Longitudinal peripheral blood (PB) samples were collected from patients with newly diagnosed chronic-phase CML enrolled in the NordCML007 (NCT01725204),[56,82] and ENEST1st (NCT01061177)[83] clinical trials. From patients ($n = 32$) in the NordML007 trial, PB samples ($N = 122$) were collected from each patient before and 1 h after the first dasatinib dose (t0, t1), and before and 1 h after dasatinib dose after 3 months of daily dasatinib treatment (t2, t3). The NordCML007 trial studied the efficacy and safety of combining dasatinib (100 mg once daily) with pegylated interferon-α2b (PegIFNα), after 3 months of dasatinib treatment. The PegIFNα was given as 15 µg/week for 3 months, then 25 µg/week for nine months. Our longitudinal sample collection was performed before the addition of PegIFNα. From patients ($n = 49$) in the ENEST1st trial treated with nilotinib (300 mg twice daily), PB samples ($N = 98$) were collected from each patient before and 3 h after the first nilotinib dose (et0, et1). Although NordCML007 and ENEST1st both enrolled newly diagnosed chronic phase CML, the inclusion and exclusion criteria were different. While the NordCML007 trial did not allow any prior treatment TKIs, and only up to 3 months of prior hydroxyurea treatment, the ENEST1st trial allowed TKI treatment for up to 3 months prior, and hydroxyurea for up to 6 months prior. The clinical demographic of the two cohorts is given in Supplementary Table 1. The levels of BCR::ABL1^{IS} the first year of TKI was comparable in the two clinical trials (Supplementary Fig. 10). All samples were preserved for mass cytometry analysis using Phosflow Lyse/Fix buffer (BD, cat# 558049) and immediately frozen in saline for long-term storage at −80 °C, as previously described.[46]

Patients in the NordCML007 and ENEST1st provided written informed consent, and the two clinical trials were approved by local ethical committees in all participating countries. The studies performed in accordance with the Declaration of Helsinki. Sampling for single-cell immune and signaling profiling was a part of the explorative biomarker program of both ENEST1st and NordCML007, and results from these analyses were explorative endpoints. PB ($n = 17$) and bone marrow (BM, $n = 19$) samples from healthy donors were collected after written informed consent (University of Bergen, Norway, ethical committee approval 2012/2247).

Barcoding

The same barcoding strategy was applied to patient samples from both trials. Up to 40 samples, including CML, HD, and technical replicates, were barcoded and pooled. To achieve this, two pools of 20 samples each were barcoded and pooled using in-house formulated 20-plex palladium reagents as described by Zunder et al.[84]. These two 20-plex barcode pools were further barcoded and pooled using two unique combinations of three cisplatin isotopes (^{194}Pt + ^{195}Pt and ^{198}Pt + ^{195}Pt), following an approach described in ref. [85] We designed the Pt barcoding such that all cells in all pools were stained with ^{195}Pt. Eosinophils take up

distinctly more ^{195}Pt than other cell types and were therefore used alongside antibody-derived cell surface marker expression during clustering and dimensionality reduction (Supplementary Text).

Single cell staining

The two master mixes of antibodies targeting cell surface markers and intracellular protein epitopes (Supplementary Table S2) were prepared prior to single-cell staining and stored in aliquots at −80 °C.[86] All barcoded sample pools from both trials were stained on the same day using the frozen antibody master mixes, according to a modified version of Standard BioTools' protocol (Maxpar Cell Surface Staining with Fresh Fix Protocol, 400276 Rev 07).

Briefly, after metal barcoding, cells were thawed, washed and incubated with heparin sodium (100 IU/mL, Wockhardt, Cat # FP1083) and FcR Blocking Reagent (1:5 dilution, Miltenyi Biotec, Cat # 130-059-901) for 20 min at room temperature to inhibit unspecific charge-based and FcR-mediated antibody binding.[49] The cells were then stained with the panel of antibodies for cell surface markers (30 min, RT), washed in cell staining buffer (CSB, SBT cat # 201068), and permeabilized with methanol (-20°C) on ice for 15 min. Further washing in CSB was followed by a second round of blocking with heparin and FcR blocking reagent. Cells were then washed in CSB and stained with the panel of antibodies for intracellular targets (30 minutes, RT). After washing, the cells were resuspended in PBS (SBT, Cat # 201058) + 4% PFA (Thermo Fisher, cat # 28906) with a 1:3000 dilution of iridium-intercalator (125 µM, SBT, cat # 201192A) and incubated overnight at 4 °C. The next day, cells were washed in CSB and frozen in FBS supplemented with 10% DMSO at −80 °C until data acquisition.[87] A pool of single-stained compensation beads was also prepared according to previously published protocols.[88]

Data acquisition

The stained and frozen barcode pools from the NordCML007 trial were thawed immediately prior to data acquisition, washed in CSB and Cell Acquisition buffer (CAS, STB, cat # 201240) and re-suspended to a final concentration of approximately 5×10^5 cells/mL in CAS containing Four element EQ Normalization beads (1:10 dilution, STB Cat # 201078). The data were acquired on a Helios mass cytometer using a wide-bore injector at an event rate of ~300 events/s. A Super Sampler (Victorian airships inc.) was used to inject cells to the mass cytometer. The single-cell sample suspensions were kept on ice during acquisition.

The stained and frozen barcode pools from the ENEST1st trial were thawed immediately prior to data acquisition, washed in CSB and Cell Acquisition buffer+ (CAS+, STB, Cat # 201244) and left pelleted in flow tubes. The flow tubes were placed in the sample carrousel of the CyTOF XT (SBT) and cell pellets were re-suspended to a final concentration of approximately 5×10^5 cells/mL in CAS+ containing Six element EQ Normalization beads (1:10 dilution, SBT, Cat # 201245) during data acquisition. The data were acquired at an event rate of ~ 300 events/s.

Pre-processing of single-cell data

The data was normalized using the Fluidigm normalizer software based on the four and six element normalization beads in single-cell data collected from samples from the NordCML007 and ENEST1st patients, respectively. The normalized data was cleaned up by manual gating using the Gaussian parameters, Event length and DNA/Ir as outlined in ref. [89]. The panel editor tool from the R package *Premessa* was used to harmonize the panels and to delete the BCKG-190 channel. The data was de-barcoded and compensated using the R package *CATALYST*. Data from acquired single-stained compensation beads was used for compensation.[88] Final removal of doublets was performed by tailored gating on CD45 vs DNA/Ir, with DNA/Ir channel set to linear. The single-cell data were not batch effect corrected.

Clustering and dimensionality reduction

Both datasets were clustered and manually annotated using the same overall two-step strategy. The first step, the main cell types were identified using Cytosplore.[50] Then, T cells, Myeloid and dendritic cells, NK cells, hematopoietic stem and progenitor cells (HSPCs) and neutrophils were re-clustered individually using PARC[51] and a tailored selection of cell surface markers (Supplementary Table S3). The same nomenclature of cell type labels was used in the annotation of clusters to enable direct comparison between datasets. Uniform Manifold Approximation and Projection for Dimensional Reduction (UMAP)[90] was used for dimensionality reduction analysis for visualization of single-cell level data.

Estimation of absolute counts from proportions

To estimate the absolute counts of different immune populations identified by mass cytometry, we multiplied the proportion of each population by the white blood cell count (WBC, 10^9/L) measured on the day of PB sampling. These estimated absolute counts were then adjusted to account for the rapid lymphocyte mobilization increasing the white blood count.[27] For details, see Supplemental Text.

Comparison of signaling in healthy donors and patient samples

We performed a group-wise comparison between healthy donors and patients before, or after three months of treatment, by calculating the difference (Δ) in mean level of each of the BCR::ABL1-related signaling pathways in each immune population for healthy donor samples and in CML patient samples. The level of BCR::ABL1 related signaling was measured in the immune populations as the 75th percentile of the hyperbolic arcsin-transformed dual counts.

Change in signaling during treatment

For each patient, to quantify the distance between cell distributions, the Earth Mover's Distance (EMD) was employed. This metric captures the minimal shift in probability mass required to align one distribution of cellular features with another, reflecting differences in their overall statistical structure. To assess the directionality of these shifts, a signed Earth Mover's Distance (sEMD) was defined by incorporating the sign of the median difference between perturbed and baseline variants.

Statistical analysis

We used the t_test() function from the R package *rstatix* to do simple two-sided Student's *t*-tests. To perform Spearman correlations, we either used the rcorr() function from the R package *Hmisc* (correlation networks), or stat_cor() from the R package *ggpubr* for simple plotting. Results from all statistical tests, including Spearman correlations, were false discovery rate adjusted using the Benjamini & Hochberg method in the p.adjust() function in base R (p_{adj}). Details on quantification of signaling ratios and sEMD is given in the Supplementary Text. We used the cv.ptLasso() function from the R package *ptLasso* to predict response to treatment from mass cytometry data. Receiver Operator Curves and Area Under the Curve (AUC) measurements was performed using the R package p*ROC*. Clusters with less than 5 cells were omitted from the statistical analysis. Welch's two-sided *t*-test was used to compare clinical parameters. We consider $p_{adj} \leq 0.05$ significant. ($p_{adj} \leq 0.05$: *, $p_{adj} \leq 0.01$: **, $p_{adj} \leq 0.001$: ***, $p_{adj} \leq 0.0001$: ****).

DATA AVAILABILITY

The preprocessed raw single cell data (.fcs files) have been deposited at Mendeley Data (https://doi.org/10.17632/jn8pg7fbbt.1) and is publicly available. Additional patient data may be made available upon reasonable request.

ACKNOWLEDGEMENTS

We acknowledge the contribution from patients and thank the work of study personnel at all study sites participating in both the NordCML007 and ENEST1st clinical trials. The single-cell data were collected using the Helios and CyTOF XT mass

cytometers at the Flow & Mass Cytometry Core Facility, Department of Clinical Science, University of Bergen. The Helios mass cytometer was funded by the Trond Mohn Research Foundation. **NordCML007:** The Norwegian University of Science and Technology (NTNU, Trondheim, Norway) sponsored the study on behalf of the Nordic CML Study Group (NCMLSG), and the trial was supported by a grant from Bristol-Myers Squibb to NTNU. **ENEST1st:** Novartis Pharmaceuticals supported the collection of blood samples for mass cytometry analysis. We acknowledge the funding from and Clinical therapy research in the specialist health services "KlinBeForsk" (project no. 2017206), Western Norway Regional Health Authority (project no. F-12846, F-12148 and F-13102) and Nordic Cancer Union (NCU).

AUTHOR CONTRIBUTIONS

Conceptualization B.T.G., and S.E.G.; Data curation B.T.G., H.H.H. D.W. and S.E.G.; Formal analysis B.T.G., and S.E.G; Funding acquisition B.T.G., H.H.H. and S.E.G.; Investigation B.T.G., H.H.H., D.W., M.H., S.M. and S.E.G.; Methodology B.T.G., and S.E.G.; Project administration B.T.G., H.H.H. D.W., and S.E.G.; Resources/Provided clinical samples and data U.O.S., J.S., J.R., T.G.D., D.W., S.M., B.T.G. and H.H.H.; Software Ø.S., M.B., E.C., R.T. and S.E.G.; Supervision B.T.G. and S.P.; Validation B.T.G., M.B., E.C., R.T.; Visualization B.T.G., M.B. and S.E.G.; Writing—original draft B.T.G and S.E.G.; Writing— review & editing all authors. All authors have read and approved the article.

FUNDING

Open access funding provided by University of Bergen.

ADDITIONAL INFORMATION

Supplementary information The online version contains supplementary material available at https://doi.org/10.1038/s41392-026-03070-z.

Competing interests: S.E.G.: Research collaboration with Novartis. H.H.H.: Chairman Nordic CML study group. Study group or institutional support from Bristol-Myers Squibb and Merck (NordCML007); Bristol Myers Squibb (DAStop 2 study), Austrian Orphan health and Pfizer (BosuPeg study); Speakers' fees: Incyte and Novartis. S.M.: Research funding from Novartis, Bristol Myers Squibb and Pfizer. B.T.G.: ENEST1st research collaboration with Novartis, collection and shipment of samples; Alden Cancer Therapy AS: Current equity holder in private company; AOP Orphan Pharmaceuticals GmbH: Consultancy; Astellas Pharma: Consultancy; AstraZeneca: Consultancy; Bjorgvin Therapeutic Group AS: Current equity holder in private company; Delbert Pharma: Consultancy; Há Biotech AS: Current equity holder in private company; Incyte: Consultancy; JAZZ Pharmaceuticals: Consultancy; Kinn Therapeutics AS: Current equity holder in private company; MSD: Consultancy; Novartis: Consultancy; Otsuka Pharma: Consultancy; Sanofi: Consultancy. M.B., E.C., M.H., Ø.S., U.O.S., J.S., J.R., T.G.D., R.T., S.P. and D.W. declare no competing interests.

Publisher's note Springer Nature remains neutral with regard to jurisdictional claims in published maps and institutional affiliations.

REFERENCES

1. Kurtz, D. M. et al. Dynamic risk profiling using serial tumor biomarkers for personalized outcome prediction. *Cell* **178**, 699–713.e19 (2019).
2. Eisenhauer, E. A. et al. New response evaluation criteria in solid tumours: revised RECIST guideline (version 1.1). *Eur. J. Cancer* **45**, 228–247 (2009).
3. Bartolomucci, A. et al. Circulating tumor DNA to monitor treatment response in solid tumors and advance precision oncology. *NPJ Precis. Oncol.* **9**, 84 (2025).
4. Nowell, P. C. The minute chromosome (Phl) in chronic granulocytic leukemia. *Blut* **8**, 65–66 (1962).
5. Rowley, J. D. Letter: A new consistent chromosomal abnormality in chronic myelogenous leukaemia identified by quinacrine fluorescence and Giemsa staining. *Nature* **243**, 290–293 (1973).
6. Daley, G. Q., Van Etten, R. A. & Baltimore, D. Induction of chronic myelogenous leukemia in mice by the P210bcr/abl gene of the Philadelphia chromosome. *Science* **247**, 824–830 (1990).
7. Cross, N. C. P. Standardisation of molecular monitoring for chronic myeloid leukaemia. *Best Pract. Res. Clin. Haematol.* **22**, 355–365 (2009).
8. Cross, N. C. P. et al. European LeukemiaNet laboratory recommendations for the diagnosis and management of chronic myeloid leukemia. *Leukemia* **37**, 2150–2167 (2023).
9. Apperley, J. F. et al. 2025 European LeukemiaNet recommendations for the management of chronic myeloid leukemia. *Leukemia* **39**, 1797–1813 (2025).
10. Hehlmann, R. et al. Assessment of imatinib as first-line treatment of chronic myeloid leukemia: 10-year survival results of the randomized CML study IV and impact of non-CML determinants. *Leukemia* **31**, 2398–2406 (2017).
11. Claudiani, S. et al. Long-term outcomes after upfront second-generation tyrosine kinase inhibitors for chronic myeloid leukemia: managing intolerance and resistance. *Leukemia* **38**, 796–802 (2024).
12. Busque, L. et al. Switching TKIs during CML therapy is frequent, mostly driven by intolerance, and does not affect survival: a prospective Quebec registry study. *Blood Cancer J.* **15**, 35 (2025).
13. Gambacorti-Passerini, C. et al. Treatment patterns and clinical outcomes of tyrosine kinase inhibitors in chronic-phase CML in clinical practice: 3-year European SIMPLICITY data. *Eur. J. Haematol.* **106**, 82–89 (2021).
14. Atallah, E. & Sweet, K. Treatment-free remission: the new goal in CML therapy. *Curr. Hematol. Malig. Rep.* **16**, 433–439 (2021).
15. Phillips, K. M. et al. Quality of life outcomes in patients with chronic myeloid leukemia treated with tyrosine kinase inhibitors: a controlled comparison. *Support. Care Cancer* **21**, 1097–1103 (2013).
16. Winn, A. N. et al. Estimated savings after stopping tyrosine kinase inhibitor treatment among patients with chronic myeloid leukemia. *JAMA Netw. Open* **6**, e2347950 (2023).
17. Chen, E. Y. et al. Loss in overall and quality-adjusted life expectancy for patients with chronic-phase chronic myeloid leukemia. *Eur. J. Haematol.* **114**, 334–342 (2025).
18. Leveque, D., Becker, G., Bilger, K. & Natarajan-Ame, S. Clinical pharmacokinetics and pharmacodynamics of dasatinib. *Clin. Pharmacokinet.* **59**, 849–856 (2020).
19. Blake, S., Hughes, T. P., Mayrhofer, G. & Lyons, A. B. The Src/ABL kinase inhibitor dasatinib (BMS-354825) inhibits function of normal human T-lymphocytes in vitro. *Clin. Immunol.* **127**, 330–339 (2008).
20. Weichsel, R. et al. Profound inhibition of antigen-specific T-cell effector functions by dasatinib. *Clin. Cancer Res.* **14**, 2484–2491 (2008).
21. Schade, A. E. et al. Dasatinib, a small-molecule protein tyrosine kinase inhibitor, inhibits T-cell activation and proliferation. *Blood* **111**, 1366–1377 (2008).
22. Huuhtanen, J. et al. IFN-alpha with dasatinib broadens the immune repertoire in patients with chronic-phase chronic myeloid leukemia. *J. Clin. Investig.* **132**, e152585 (2022).
23. Mustjoki, S. et al. Clonal expansion of T/NK-cells during tyrosine kinase inhibitor dasatinib therapy. *Leukemia* **23**, 1398–1405 (2009).
24. Kreutzman, A. et al. Immunological monitoring of newly diagnosed CML patients treated with bosutinib or imatinib first-line. *Oncoimmunology* **8**, e1638210 (2019).
25. Chang, M. C. et al. NKG2A down-regulation by dasatinib enhances natural killer cytotoxicity and accelerates effective treatment responses in patients with chronic myeloid leukemia. *Front. Immunol.* **9**, 3152 (2018).
26. Marcos-Jimenez, A. et al. Dasatinib-induced spleen contraction leads to transient lymphocytosis. *Blood Adv.* **7**, 2418–2430 (2023).
27. Mustjoki, S. et al. Rapid mobilization of cytotoxic lymphocytes induced by dasatinib therapy. *Leukemia* **27**, 914–924 (2013).
28. Colom-Fernandez, B. et al. Immediate effects of dasatinib on the migration and redistribution of naive and memory lymphocytes associated with lymphocytosis in chronic myeloid leukemia patients. *Front. Pharmacol.* **10**, 1340 (2019).
29. Tanaka, C. et al. Clinical pharmacokinetics of the BCR-ABL tyrosine kinase inhibitor nilotinib. *Clin. Pharmacol. Ther.* **87**, 197–203 (2010).
30. Manley, P. W. et al. Extended kinase profile and properties of the protein kinase inhibitor nilotinib. *Biochim. Biophys. Acta* **1804**, 445–453 (2010).
31. Fei, F. et al. Effects of nilotinib on regulatory T cells: the dose matters. *Mol. Cancer* **9**, 22 (2010).
32. Dorfel, D. et al. The BCR-ABL inhibitor nilotinib influences phenotype and function of monocyte-derived human dendritic cells. *Cancer Immunol. Immunother.* **67**, 775–783 (2018).
33. Bellora, F. et al. Imatinib and nilotinib off-target effects on human NK cells, monocytes, and M2 macrophages. *J. Immunol.* **199**, 1516–1525 (2017).
34. Karabay, A. Z. et al. Nilotinib exhibits less toxicity than imatinib and influences the immune state by modulating iNOS, p-p38 and p-JNK in LPS/IFN gamma-activated macrophages. *Toxicol. In Vitro* **95**, 105754 (2024).
35. Graham, S. M. et al. Primitive, quiescent, Philadelphia-positive stem cells from patients with chronic myeloid leukemia are insensitive to STI571 in vitro. *Blood* **99**, 319–325 (2002).
36. Copland, M. et al. Dasatinib (BMS-354825) targets an earlier progenitor population than imatinib in primary CML but does not eliminate the quiescent fraction. *Blood* **107**, 4532–4539 (2006).
37. Hamilton, A. et al. Chronic myeloid leukemia stem cells are not dependent on Bcr-Abl kinase activity for their survival. *Blood* **119**, 1501–1510 (2012).
38. Corbin, A. S. et al. Human chronic myeloid leukemia stem cells are insensitive to imatinib despite inhibition of BCR-ABL activity. *J. Clin. Investig.* **121**, 396–409 (2011).
39. Gullaksen, S. E. et al. CML stem cells and their interactions and adaptations to tyrosine kinase inhibitors. *Leuk. Lymphoma* **66**, 1211–1220 (2025).

40. Bocchia, M. et al. Residual peripheral blood CD26(+) leukemic stem cells in chronic myeloid leukemia patients during TKI therapy and during treatment-free remission. *Front. Oncol.* **8**, 194 (2018).
41. Chomel, J. C. et al. Leukemic stem cell persistence in chronic myeloid leukemia patients in deep molecular response induced by tyrosine kinase inhibitors and the impact of therapy discontinuation. *Oncotarget* **7**, 35293–35301 (2016).
42. Mustjoki, S. et al. Impact of malignant stem cell burden on therapy outcome in newly diagnosed chronic myeloid leukemia patients. *Leukemia* **27**, 1520–1526 (2013).
43. Schultheis, B., Szydlo, R., Mahon, F. X., Apperley, J. F. & Melo, J. V. Analysis of total phosphotyrosine levels in CD34+ cells from CML patients to predict the response to imatinib mesylate treatment. *Blood* **105**, 4893–4894 (2005).
44. White, D. et al. Measurement of in vivo BCR-ABL kinase inhibition to monitor imatinib-induced target blockade and predict response in chronic myeloid leukemia. *J. Clin. Oncol.* **25**, 4445–4451 (2007).
45. Iriyama, N., Hatta, Y. & Takei, M. Direct effect of dasatinib on signal transduction pathways associated with a rapid mobilization of cytotoxic lymphocytes. *Cancer Med.* **5**, 3223–3234 (2016).
46. Gullaksen, S. E. et al. Single cell immune profiling by mass cytometry of newly diagnosed chronic phase chronic myeloid leukemia treated with nilotinib. *Haematologica* **102**, 1361–1367 (2017).
47. Omsland, M. et al. Tyrosine kinase inhibitors and interferon-alpha increase tunneling nanotube (TNT) formation and cell adhesion in chronic myeloid leukemia (CML) cell lines. *FASEB J* **34**, 3773–3791 (2020).
48. Geelen, I. G. P. et al. Switching from imatinib to nilotinib plus pegylated interferon-alpha2b in chronic phase CML failing to achieve deep molecular response: clinical and immunological effects. *Ann. Hematol.* **102**, 1395–1408 (2023).
49. Rahman, A. H., Tordesillas, L. & Berin, M. C. Heparin reduces nonspecific eosinophil staining artifacts in mass cytometry experiments. *Cytometry A.* **89**, 601–607 (2016).
50. van Unen, V. et al. Visual analysis of mass cytometry data by hierarchical stochastic neighbour embedding reveals rare cell types. *Nat. Commun.* **8**, 1740 (2017).
51. Stassen, S. V. et al. PARC: ultrafast and accurate clustering of phenotypic data of millions of single cells. *Bioinformatics* **36**, 2778–2786 (2020).
52. Gustafson, M. P., Lin, Y., Ryder, M. & Dietz, A. B. Strategies for improving the reporting of human immunophenotypes by flow cytometry. *J. Immunother. Cancer* **2**, 18 (2014).
53. Panopoulos, A. D. et al. STAT3 governs distinct pathways in emergency granulopoiesis and mature neutrophils. *Blood* **108**, 3682–3690 (2006).
54. Sneed, T. B. et al. The significance of myelosuppression during therapy with imatinib mesylate in patients with chronic myelogenous leukemia in chronic phase. *Cancer* **100**, 116–121 (2004).
55. Cortes, J. E. et al. Final 5-year study results of DASISION: the dasatinib versus imatinib study in treatment-naive chronic myeloid leukemia patients trial. *J. Clin. Oncol.* **34**, 2333–2340 (2016).
56. Hjorth-Hansen, H. et al. Safety and efficacy of the combination of pegylated interferon-alpha2b and dasatinib in newly diagnosed chronic-phase chronic myeloid leukemia patients. *Leukemia* **30**, 1853–1860 (2016).
57. Warfvinge, R. et al. Single-cell molecular analysis defines therapy response and immunophenotype of stem cell subpopulations in CML. *Blood* **129**, 2384–2394 (2017).
58. Sadovnik, I. et al. Expression of CD25 on leukemic stem cells in BCR-ABL1(+) CML: potential diagnostic value and functional implications. *Exp. Hematol.* **51**, 17–24 (2017).
59. Schafranek, L. et al. Sustained inhibition of STAT5, but not JAK2, is essential for TKI-induced cell death in chronic myeloid leukemia. *Leukemia* **29**, 76–85 (2015).
60. Ilaria, R. L. Jr & Van Etten, R. A. P210 and P190(BCR/ABL) induce the tyrosine phosphorylation and DNA binding activity of multiple specific STAT family members. *J. Biol. Chem.* **271**, 31704–31710 (1996).
61. Evrard, M. et al. Developmental analysis of bone marrow neutrophils reveals populations specialized in expansion, trafficking, and effector functions. *Immunity* **48**, 364–379.e8 (2018).
62. Zhu, Y. P. et al. Identification of an early unipotent neutrophil progenitor with pro-tumoral activity in mouse and human bone marrow. *Cell Rep* **24**, 2329–2341.e8 (2018).
63. Zhu, Y. P. et al. CyTOF mass cytometry reveals phenotypically distinct human blood neutrophil populations differentially correlated with melanoma stage. *J. Immunother. Cancer* **8**, e000473 (2020).
64. Craig, E. et al. Pretraining and the lasso. *J. R. Stat. Soc. Ser. B Stat. Methodol.* **88**, 261–281 (2026).
65. Varma, S. & Simon, R. Bias in error estimation when using cross-validation for model selection. *BMC Bioinformatics* **7**, 91 (2006).
66. Irish, J. M. et al. Single cell profiling of potentiated phospho-protein networks in cancer cells. *Cell* **118**, 217–228 (2004).
67. Tislevoll, B. S. et al. Early response evaluation by single-cell signaling profiling in acute myeloid leukemia. *Nat. Commun.* **14**, 115 (2023).
68. Kantarjian, H. et al. Dasatinib versus imatinib in newly diagnosed chronic-phase chronic myeloid leukemia. *N. Engl. J. Med.* **362**, 2260–2270 (2010).
69. Saglio, G. et al. Nilotinib versus imatinib for newly diagnosed chronic myeloid leukemia. *N. Engl. J. Med.* **362**, 2251–2259 (2010).
70. Matsumura, I. et al. Nilotinib vs dasatinib in achieving MR4.5 for de novo chronic myeloid leukemia: the randomized JALSG CML212 study. *Blood Adv.* **8**, 5237–5247 (2024).
71. Klumpen, H. J., Samer, C. F., Mathijssen, R. H., Schellens, J. H. & Gurney, H. Moving towards dose individualization of tyrosine kinase inhibitors. *Cancer Treat. Rev.* **37**, 251–260 (2011).
72. Hughes, A. et al. CML patients with deep molecular responses to TKI have restored immune effectors and decreased PD-1 and immune suppressors. *Blood* **129**, 1166–1176 (2017).
73. Bruck, O. et al. Immune cell contexture in the bone marrow tumor microenvironment impacts therapy response in CML. *Leukemia* **32**, 1643–1656 (2018).
74. Ilander, M. et al. Enlarged memory T-cell pool and enhanced Th1-type responses in chronic myeloid leukemia patients who have successfully discontinued IFN-alpha monotherapy. *PLoS One* **9**, e87794 (2014).
75. Harrington, P. et al. Differential inhibition of T-cell receptor and STAT5 signaling pathways determines the immunomodulatory effects of dasatinib in chronic phase chronic myeloid leukemia. *Haematologica* **108**, 1555–1566 (2023).
76. Salih, J. et al. The BCR/ABL-inhibitors imatinib, nilotinib and dasatinib differentially affect NK cell reactivity. *Int. J. Cancer* **127**, 2119–2128 (2010).
77. Kuepper, M. K. et al. Stem cell persistence in CML is mediated by extrinsically activated JAK1-STAT3 signaling. *Leukemia* **33**, 1964–1977 (2019).
78. Patel, S. B. et al. Metabolic alterations mediated by STAT3 promotes drug persistence in CML. *Leukemia* **35**, 3371–3382 (2021).
79. Shanmuganathan, N. et al. Early BCR-ABL1 kinetics are predictive of subsequent achievement of treatment-free remission in chronic myeloid leukemia. *Blood* **137**, 1196–1207 (2021).
80. Anensen, N. et al. A distinct p53 protein isoform signature reflects the onset of induction chemotherapy for acute myeloid leukemia. *Clin. Cancer Res.* **12**, 3985–3992 (2006).
81. Gausdal, G. et al. Abolition of stress-induced protein synthesis sensitizes leukemia cells to anthracycline-induced death. *Blood* **111**, 2866–2877 (2008).
82. Flygt, H. et al. Long-term tolerability and efficacy after initial PegIFN-alpha addition to dasatinib in CML-CP: five-year follow-up of the NordCML007 study. *Eur. J. Haematol.* **107**, 617–623 (2021).
83. Hochhaus, A. et al. Frontline nilotinib in patients with chronic myeloid leukemia in chronic phase: results from the European ENEST1st study. *Leukemia* **30**, 57–64 (2016).
84. Zunder, E. R. et al. Palladium-based mass tag cell barcoding with a doublet-filtering scheme and single-cell deconvolution algorithm. *Nat. Protoc.* **10**, 316–333 (2015).
85. McCarthy, R. L., Mak, D. H., Burks, J. K. & Barton, M. C. Rapid monoisotopic cisplatin based barcoding for multiplexed mass cytometry. *Sci. Rep.* **7**, 3779 (2017).
86. Schulz, A. R. et al. Stabilizing antibody cocktails for mass cytometry. *Cytometry A* **95**, 910–916 (2019).
87. Sumatoh, H. R., Teng, K. W., Cheng, Y. & Newell, E. W. Optimization of mass cytometry sample cryopreservation after staining. *Cytometry A* **91**, 48–61 (2017).
88. Chevrier, S. et al. Compensation of signal spillover in suspension and imaging mass cytometry. *Cell Syst.* **6**, 612–620.e5 (2018).
89. Bagwell, C. B. et al. Automated data cleanup for mass cytometry. *Cytometry A* **97**, 184–198 (2020).
90. McInnes, L., Healy, J. & Melville, J. UMAP: uniform manifold approximation and projection for dimension reduction. Preprint at https://arxiv.org/abs/1802.03426 (2018).

Open Access This article is licensed under a Creative Commons Attribution 4.0 International License, which permits use, sharing, adaptation, distribution and reproduction in any medium or format, as long as you give appropriate credit to the original author(s) and the source, provide a link to the Creative Commons licence, and indicate if changes were made. The images or other third party material in this article are included in the article's Creative Commons licence, unless indicated otherwise in a credit line to the material. If material is not included in the article's Creative Commons licence and your intended use is not permitted by statutory regulation or exceeds the permitted use, you will need to obtain permission directly from the copyright holder. To view a copy of this licence, visit http://creativecommons.org/licenses/by/4.0/.

© The Author(s) 2026